Optica Applicata, Vol. XLI, No. 1, 2011

Optical and electrical characterization of reverse bias luminescence in InGaN light emitting diodes

HSIANG CHEN[1*], CHYUAN-HAUR KAO[2], TIEN-CHANG LU[3], SHIH-CHANG SHEI[4]

[1]Department of Applied Materials and Optoelectronic Engineering, National Chi Nan University, Puli, Taiwan, R.O.C.

[2]Department of Electronic Engineering, Chang Gung University, Kwei-Shan, Taiwan, R.O.C.

[3]Department of Photonics, National Chiao Tung University, Hsinchu, Taiwan, R.O.C.

[4]Department of Electrical Engineering, National University of Tainan, Tainan, Taiwan, R.O.C.

[*]Corresponding author: hchen@ncnu.edu.tw

This study investigates the reliability physics of the reverse bias luminescence (RBL) of InGaN/GaN light emitting diodes. Optical and electrical characterization techniques including surface temperature measurements, 2D X-ray fluorescent element analysis, and 2D electroluminescence (EL) measurements reveal the leakage current distribution and the origin of the reverse bias leakage current. Using these techniques, this study examines the electroluminescence behavior and surface temperature distribution in forward bias and reverse bias conditions. Results show that the reverse bias EL originates from hot electron-induced emission, which in turn is due to the leakage current in the high electric field region caused by metal contact abnormalities. The optical and electrical characterization techniques adopted in this study are a promising screening tool for correlating device failures with fabrication processes.

Keywords: GaN LED, electroluminescence, reverse-bias, leakage current, hot carrier.

1. Introduction

Research on GaN LED technology over the past decade has developed full-color indicators and full-color displays. However, reliability problems caused by leakage current may limit the future industrial applications of GaN LEDs [1]. This paper uses nondestructive optical characterization, electrical measurements, and reverse bias electroluminescence observations to investigate the reliability of InGaN LEDs. The traditional approach to investigating the defect structures requires destructive techniques [2]. For industrial applications, however, devices cannot be sacrificed

during testing. Therefore, it is necessary to develop optical device characterization techniques to examine the material and electrical properties of InGaN LEDs for future industrial applications. Since the optical and electrical characterization of GaN has been well established in electronic devices [3] and silicon capacitors [4], this study extends the scope of nondestructive optical screening techniques to GaN optoelectronic devices such as LEDs and lasers. Specifically, this study uses optical characterization techniques, surface temperature measurements, and 2D electroluminescence (EL) measurements to detect device abnormality. X-ray fluorescent (XRF) element analysis can reveal the internal composition of a device and locate any abnormalities. Combining optical and electrical characterization techniques can help visualize reverse bias luminescence (RBL) in the high electric field region and metal contact abnormality related to the leakage current. This approach provides insights regarding the origin of the instability issue.

2. Instrument setup and device fabrication

Figure 1 illustrates the optical characterization systems above. Since these three optical characterization systems all measure the light emitted from a device, Fig. 1 uses a single graph to depict their functions. For the EL detection system, the experiments in this study biased the device under a forward bias and reverse bias and then measured the visible and NIR light emission (0.3 μm to 1 μm wavelength range). Then, analyzing the IR radiation (3 μm to 4 μm wavelength range), using an IR imager system [5], produces 2D surface temperature images of the biased device. An XRF element analysis system uses a similar optical system, including an X-ray excitation source, to collect and analyze the stimulated X-ray radiation from the device and ultimately produce clear 2D element distribution images of the device. A combination of EL observation, surface temperature measurement, 2D element distribution, and electrical

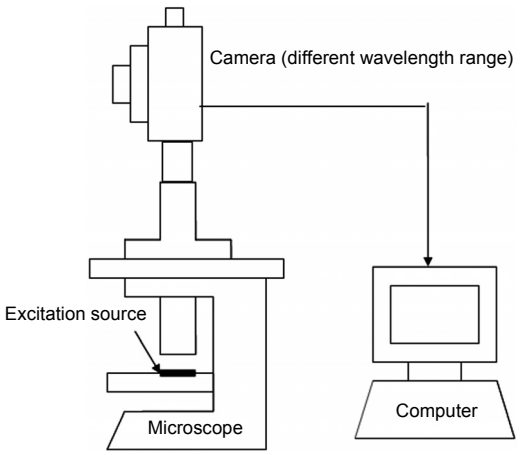

Fig. 1. The graph of the three optical characterization systems.

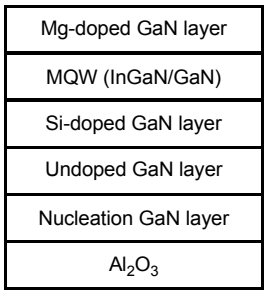

Fig. 2. Device structure.

measurement can reveal the leakage current caused by structural abnormalities without damaging the device.

The InGaN/GaN MQW LEDs are grown by metal organic chemical vapor deposition (MOCVD) on a *c*-face 2-inch sapphire (0001) substrate. The device structure consists of a 30 nm GaN nucleation layer, a Si-doped *n*-type GaN buffer layer, a 50 nm Mg-doped electron blocking layer, and a Mg-doped *p*-GaN layer. InGaN/GaN quantum well-barrier pairs are stacked between the *p*-type GaN and the *n*-type GaN layers. After the sample is partially etched down to n^+ layer, a 230 nm surface indium-tin oxide (ITO) layer is deposited onto the sample surface to function as the transparent contact layer (TCL). Besides, Ti/Al/Ti/Au contact is evaporated onto the exposed *n*-type GaN layer to function as the *n*-type electrode. The device structure is shown as Fig. 2.

3. Results and discussion

Since hot carriers do not induce reverse bias emission specific to certain types of LED devices, this study uses two types of devices to examine the phenomenon in a more detailed and quantitative way. This approach reveals the relationship between luminescence behavior and device performance.

To analyze the compositions of a device, this study uses the 2D XRF element analysis to find the 2D distribution of different composite elements. XRF is a powerful tool for detecting elements on the periodic table between Na (atomic number 11) and U (atomic number 92). By detecting the fluorescent light stimulated from X-rays, XRF can clearly present the composite elements of the chip in 2D images. For packed LED devices with a resin coating or white light LED devices with a phosphorus layer, XRF scanning can penetrate the resin coating or the phosphor layer because its scan depth is approximately 5 mm for non-metal materials. However, the scan depth for metal is less than 50 μm. As Figure 3 shows, X-rays can penetrate all the layers on top of the metal layer in the first type of LED chip, but not the metal layer. Therefore, XRF analysis can clearly identify the edge of the metal contact or the border between the chip area and the metal contact.

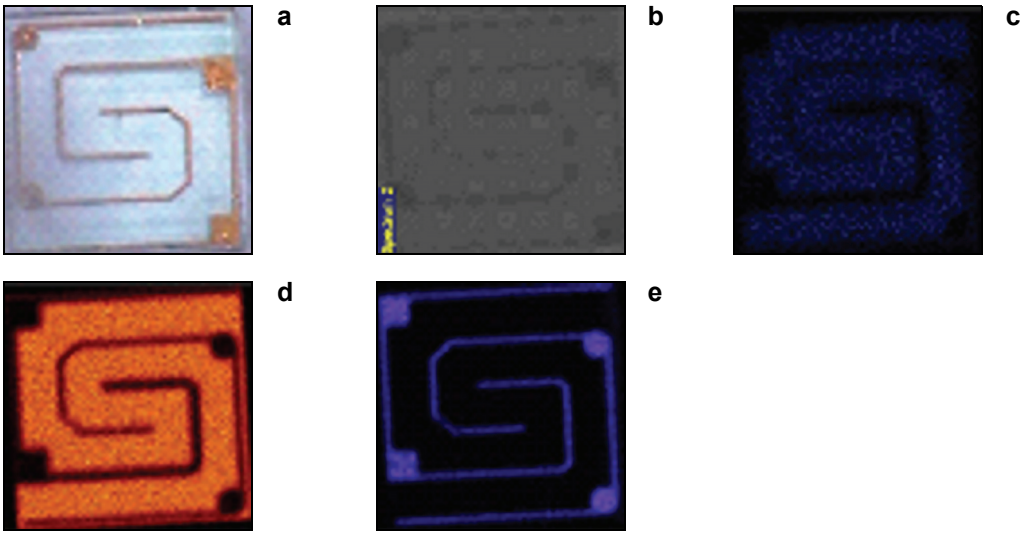

Fig. 3. A top view photo of the device (**a**). XRF analysis: X-ray image (**b**), In (**c**), Ga (**d**), Au (**e**). (The concentration is proportional to the light intensity.)

Figure 3**a** shows a top view photo of the first type device. Figure 3**b** shows an X-ray stimulated image of the LED chip from 2D XRF element analysis. By analyzing the X-ray emission spectrum at each point, Figs. 3**c**, 3**d**, and 3**e** show the indium distribution, gallium distribution, and gold distribution. These images reveal gold in the two electrode lines and the edge between the chip area and the metal contact.

LED devices functioning as semiconductor light sources usually operate under forward bias conditions. Several researchers have recently studied the instability of GaN LEDs by observing the device behavior during reverse bias operations [6]. The reverse bias operation of InGaN LEDs sheds some light on device reliability problems by revealing the high electric field regions and the reverse bias leakage current caused by contact abnormalities. These abnormalities may affect the electrical properties of InGaN LED devices.

To understand the high electric field region and the reverse bias leakage current during device operations, this study measures LED chip surface temperature under forward bias and reverse bias conditions, as Figs. 4**a** and 4**b** show. This study measures device surface temperature distributions using an IR imager. Figure 4**a** shows that high current due to band-to-band recombination creates a high temperature area on the surface of a device under forward bias conditions [5]. The higher the current is, the greater the power dissipation and temperature will be. Compared with the forward bias condition, the electrode area is hotter than the chip area. This indicates that the reverse bias condition may produce a higher leakage current and electric field, heating up the electrode. This is because high power dissipation leads to a high temperature, and the power dissipation rate equals the amount of the voltage drop

timing the current. However, the temperature difference of 10 °C between the chip area and the electrode area in the reverse bias condition is much less than the difference of 40 °C in the forward bias condition, showing that the leakage current of LED chips is small compared to the recombination current.

To observe device abnormalities during operation, this study investigates electroluminescence behavior under forward bias and reverse bias conditions for two types of devices. While band-to-band recombination is responsible for light emission during forward bias operations, the reverse bias emission may produce hot electron emission or yellow luminescence. Since the reverse bias leakage current is much smaller than the forward bias recombination current, a device under forward bias conditions can generate much stronger band-to-band recombination light emission than the leakage current-induced emission during reverse bias operation. Therefore, compared with the forward bias EL emission, the reverse bias EL emission is nearly

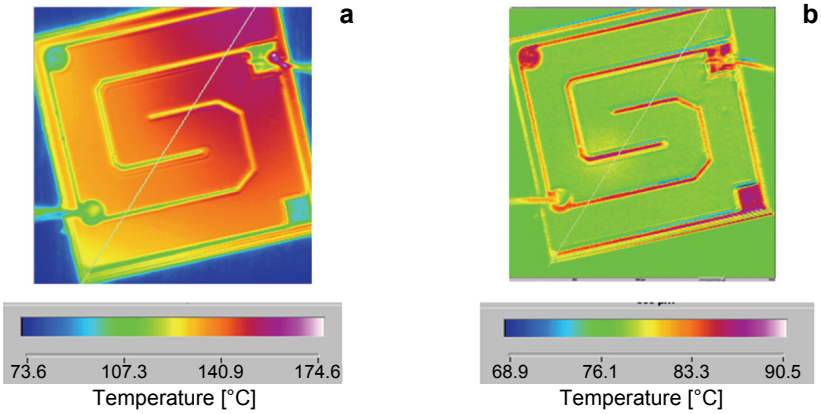

Fig. 4. Surface temperature measurements of a device with forward bias (**a**), and with reverse bias (**b**).

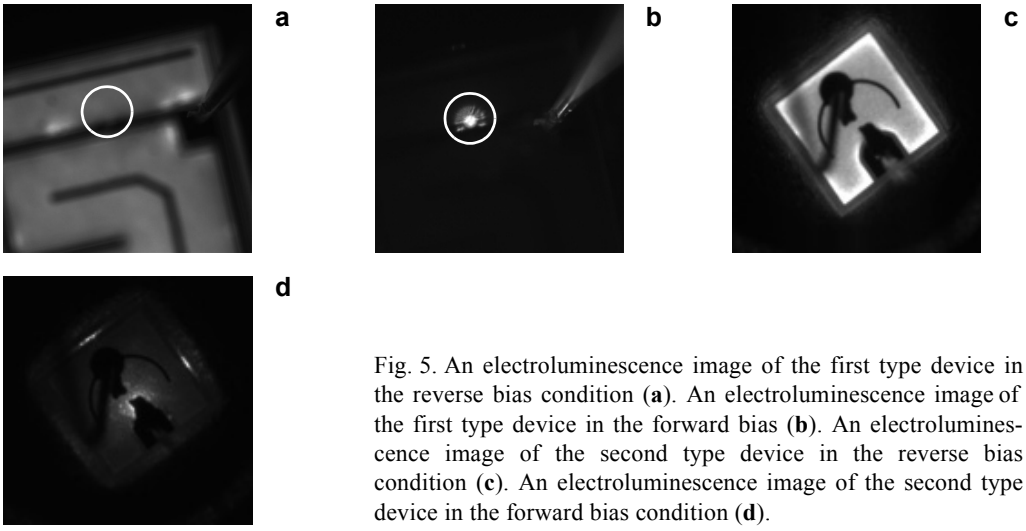

Fig. 5. An electroluminescence image of the first type device in the reverse bias condition (**a**). An electroluminescence image of the first type device in the forward bias (**b**). An electroluminescence image of the second type device in the reverse bias condition (**c**). An electroluminescence image of the second type device in the forward bias condition (**d**).

undetectable. The experiment in this study used a high-resolution cooled iXON EMCCD camera to collect the weak light emission from the device under reverse bias conditions. The first type device exhibited a weak emission spot near the border of the chip and the electrode. Figures 5**a** and 5**b** show that no forward bias light emission comes from the spot area. Compared with the first device, Fig. 5**c** shows that the forward bias emission in the second device comes from the chip area. Figure 5**d** shows that the spot-like reverse bias emission occurs in the central chip area and the line-like reverse bias emission occurs in the edge area. Moreover, while the luminance area is less than 1% of the chip area for the first type device, the emission area reaches 20% for the second type device.

This study analyzes the reverse bias emission area using a comparison of the forward bias emission, reverse bias emission, and element analysis images in superposition images. Figure 6**a** compares the forward bias EL (white) and reverse bias EL (red) areas in the type device using a superposition image. The reverse bias

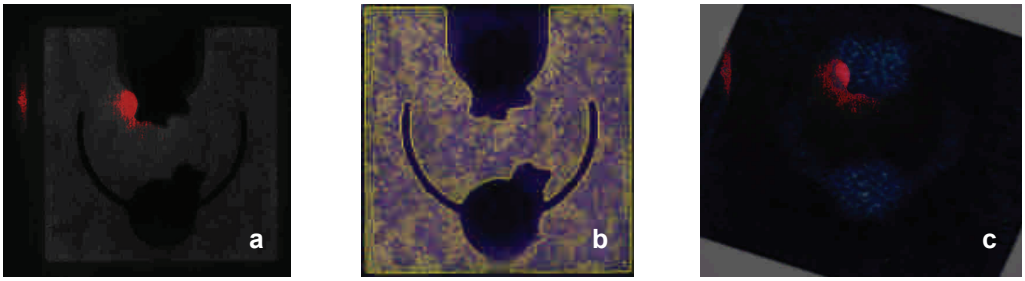

Fig. 6. Comparison of forward bias EL (luminescence area) and reverse bias EL (in red) areas in the second type device in the superposition image (**a**). Comparison of forward bias EL (in yellow) and Ga distribution (in purple) areas in the second type device in the superposition image (**b**). Comparison of forward bias EL (in yellow) and Ga XRF distribution (in purple) areas in the second type device in the superposition image. Comparison of reverse bias EL (in red) and Ga distribution (in purple) areas in the second type device in the superposition image. Comparison of reverse bias EL (in red) and Au XRF distribution (in blue) areas in the second type device in the superposition image (**c**).

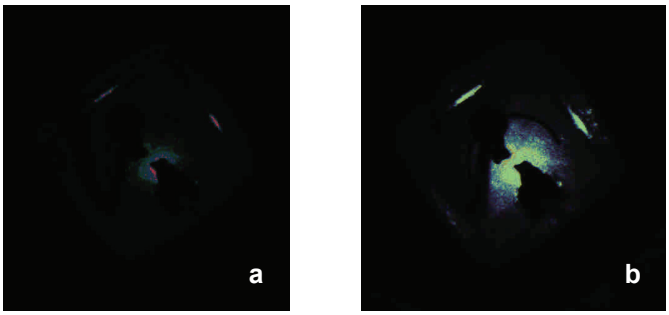

Fig. 7. The enlarged reverse bias EL area with different bias voltages (V = –8 V, pink; V = –9 V, blue; V = –9.5 V, green) – **a**. The enlarged reverse bias EL area with different bias voltages (V = –10 V, yellow; V = –11 V, green-blue; V = –12 V, purple) – **b**.

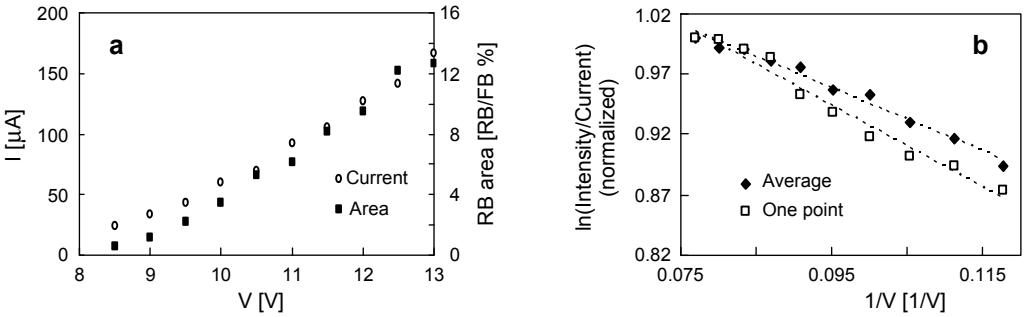

Fig. 8. The reverse bias leakage current versus the reverse bias voltage and the reverse bias emission area percentage over the whole chip versus the reverse bias voltage (**a**). The graph of the nature logarithm of the light intensity from one point and the average light intensity from the whole chip divided by the intensity versus the reciprocal of the applied voltage (**b**).

emission area appears in the border of the forward bias emission area close to the non-emission area. The two superposition images Figs. 6**b** and 6**c** compare the forward bias EL and Ga XRF distribution areas (the chip area) and reverse bias EL and Au XRF distribution areas (the metal contact) in the second type device. Figure 6**b** shows that the forward bias emission area covers the gallium rich area except for the near contact area, while the reverse bias emission occurs in the metal contact and the chip overlap area. The line-like reverse bias emission occurs in the square edge of circumference. Figure 6**c** shows that this emission also appears in the metal area outside the chip.

To investigate the reverse bias emission mechanism quantitatively, this study explores the relationship between emission area, emission intensity, leakage current distribution, and electric field. Figures 7**a** and 7**b** show that the reverse bias emission area increases as the negative voltage increases during reverse bias operations in the second type of device. Figure 8 shows that the increase rate of the reverse bias emission area is close to the increase rate of the leakage current. This suggests that current-induced EL (hot-carrier induced EL) may be the mechanism of the luminescence because the stronger the leakage current is, the larger the leakage current-induced emission area will be.

Hot electron-induced luminescence equation:

$$\text{Light intensity} \propto I \exp\left(-\frac{\varphi}{\lambda E_m}\right) \tag{1}$$

Based on previous studies, hot electron-induced emission or yellow luminescence may cause reverse bias emission [7]. However, the yellow luminescence mechanism should be excluded in this case. This is because yellow electroluminescence is not hot [8], and the reverse EL spot is around the high temperature area, as Fig. 4**b** indicates. Therefore, the reverse bias emission is likely due to hot electron-induced emission. In the hot electron-induced emission in Eq. (1), I is the current, λ is the mean

free path, φ is the loss of kinetic energy, and E_m is the maximum electric field [9, 10]. The light emission intensity is proportional to the leakage current and exponentially proportional to the negative reciprocal of the electric field. The experiment in this study measures reverse bias luminescence intensity, leakage current, and electric field (reverse bias voltage). The relationship between these factors fits the hot electron--induced luminescence equation, as the graph of the natural logarithm of the light intensity divided by the intensity versus the reciprocal of the applied voltage (shown in Fig. 8**b**) is close to a straight line with a negative slope corresponding to Eq. (1). These results confirm the hot electron-induced emission mechanism of the reverse bias emission. Thus, the reverse bias emission may imply the presence of a local high electric field. The deformation of the electrode metal [11] may cause a local high electric field to generate the emission.

Finally, this study examines the influence of the reverse bias emission spot on the electrical characteristics of the first and second devices, and measures the I–V curves using an HP 4145. Figure 9**a** shows the I–V curves of the first device with and without the RBL spot. Under the forward bias condition, the difference between the forward conduction current in the subthreshold region and the fully turned-on mode between the device with RBL spot and the device without the spot is less than 10%. According to the enlarged view of the I–V curve in the reverse bias condition in Fig. 5**b**, the device with the spot has a stronger reverse bias current than the device without the spot. For example, when a reverse bias voltage of 10 V is applied to the device, the current of the device with the spot is 9.1 μA, which is about 1.4 times of that of the device without the spot. For the first type of device, the RBL spot does not significantly contribute to a leakage current difference. Since the luminance area is less than 1% of the chip area and the reverse bias leakage current difference is less than 10%, this study compares the first device to the second device. In the second type of device, the difference between devices with and without RBL is much more distinct. The RBL emission area exceeds 20% of the chip area during high negative operations, and the reverse bias leakage current difference between the device with and without RBL is more than 10000 times. Figure 9**c** shows the I–V curves of the second device with and without RBL. Figure 9**d** shows an enlarged view of the reverse bias conditions, while Fig. 9**e** shows an enlarged view of the subthreshold region under forward bias conditions. For two devices with different RBL characteristics but the same reverse bias voltage of –10 V, Fig. 9**d** shows that the leakage current of the device with RBL is about 100 μA, while the leakage current of the device with no light emission has a leakage current of 5 nA. While the RBL spot in the first type device does not make much difference in the forward conduction current in the subthreshold region under forward bias conditions, Fig. 9**e** shows that the leakage current varies drastically between second type devices with different reverse bias emission characteristics in the subthreshold region during the forward bias. The second type of device with reverse bias light emission has a subthershold current 500 times

greater than the device without light emission. In the fully turned-on region, the leakage current effect is not as obvious because the strong forward band-to-band recombination current between the two devices with and without RBL is similar (less than 10%). Though the leakage current difference cannot be detected due to the masking effect of the band-to-band recombination current, it is still present and may damage the device.

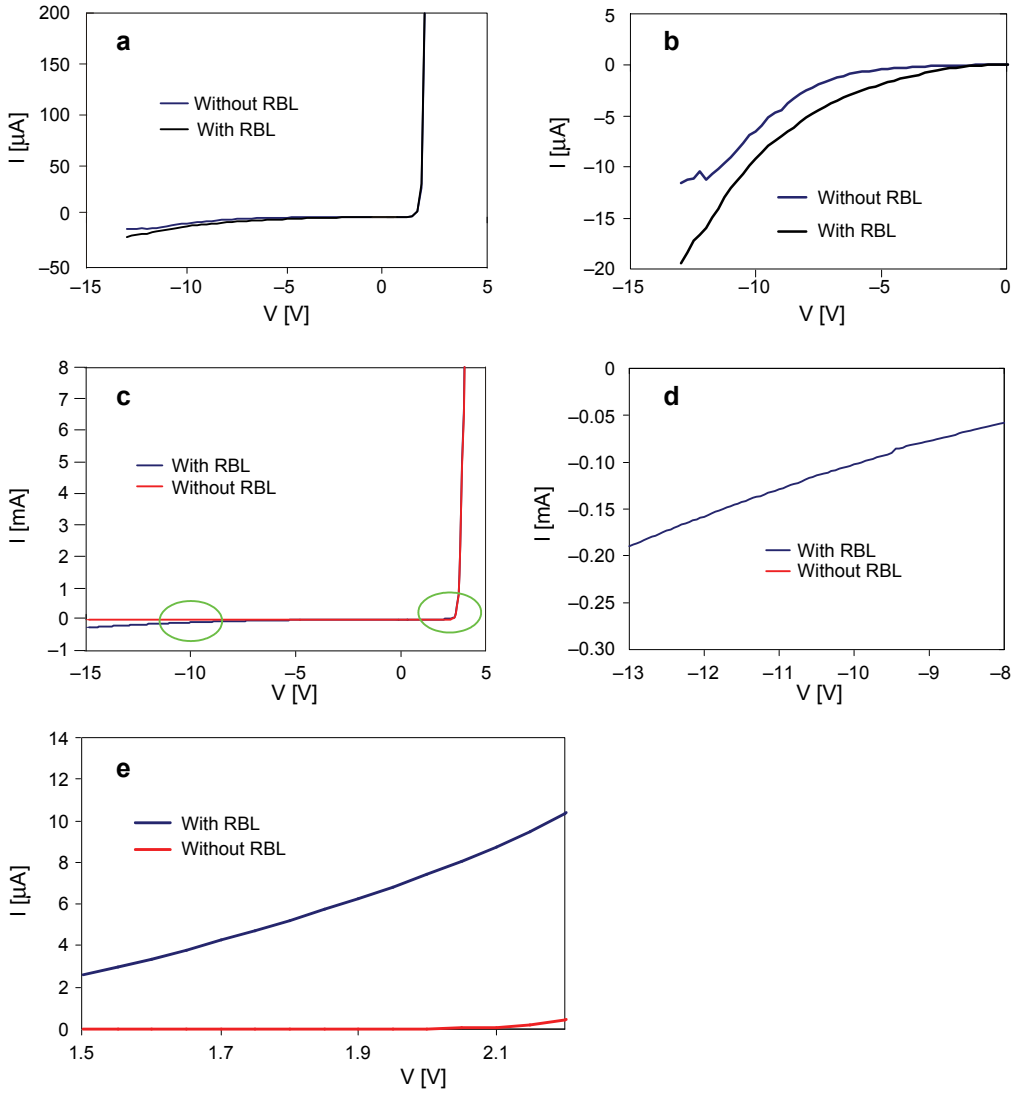

Fig. 9. The *I–V* curve of the first type of device with and without RBL (**a**). The enlarged view of (**a**) under reverse bias (**b**). The *I–V* curves of the second type device with and without RBL (**c**). The enlarged view of (**c**) under reverse bias (**d**). The enlarged view of (**c**) in the subthreshold region under forward bias (**e**).

Since a high electric field created by imperfect metal contact may drastically influence the leakage current both in the reverse bias and the forward bias conditions, the leakage current effect may deteriorate LED performance after a long period of operation.

4. Conclusions

This study investigates the reverse bias electroluminescence related to leakage current in InGaN LEDs. This study uses optical and electrical characterization techniques including XRF element analysis, EL observations, surface temperature profiles, and *I-V* measurements to examine the high electric field region created by metal contact abnormalities. The reverse bias EL originates from hot electron-induced emission from the leakage current. Because reverse bias EL is vulnerable to hot electron-induced degradation, a combination of XRF analysis and reverse bias EL observation can assess device quality. XRF can identify the edges or borders of the metal area in newly manufactured LED devices, especially for devices with an unknown fabrication process. This study uses the reverse bias EL test to identify the location of noticeable leakage current from the edge or border of the metal and the chip area. This study assesses device quality just like plumbers use soapy water to find the location of the gas leak from the pipes. The proposed techniques are promising screening tools for correlating device failures with fabrication processes.

Acknowledgements – This work was supported by the National Science Council, Taiwan, Republic of China, under Contract No. NSC-98-2221-E-260-006.

References

[1] CAO X.A., TEETSOVA J.A., SHAHEDIPOUR-SANDVIK F., ARTHUR S.D., *Microstructural origin of leakage current in GaN/InGaN light-emitting diodes*, Journal of Crystal Growth **264**(1–3), 2004, pp. 172–177.

[2] SUN Y., YU T., ZHAO H., SHAN X., ZHANG X., CHEN Z., KANG X., YU D., ZHANG G., *Microanalyses of the reverse bias leakage current increase in the laser lift off GaN-based light emitting diodes*, Journal of Applied Physics **106**(1), 2009, p. 013101.

[3] CHEN H., *Exploration of the Potential Defects in GaN HEMTs*, Verlag Dr. Müller, Saarbrücken, Germany, 2009.

[4] KAO C.H., CHEN H., CHIU J.S., CHEN K.S., PAN Y.T., *Physical and electrical characteristics of the high-k Ta_2O_5 (tantalum pentoxide) dielectric deposited on the polycrystalline silicon*, Applied Physics Letters **96**(11), 2010, p. 112901.

[5] CHEN H., PREECHA P., LAI Z., LI G.P., *Investigation of anomaly in GaN HEMTs*, Journal of the Electrochemical Society **155**(9), 2008, pp. H648–H652.

[6] CHEN N.C., WANG Y.N., WANG Y.S., LIEN W.C., CHEN Y.C., *Damage of light-emitting diodes induced by high reverse bias stress*, Journal of Crystal Growth **311**(3), 2009, pp. 994–997.

[7] KIKAWA J., YOSHIDA S., ITOH Y., *Electroluminescence studies under forward and reverse bias conditions of nitride-rich $GaN_{1-x}P_x$ SQW structure LED grown by laser-assisted metal-organic chemical vapor deposition*, Solid-State Electronics **47**(3), 2003, pp. 523–527.

[8] CHEN H., LAI Z., KUNG S.C., PENNER R.M., CHOU Y.C., LAI R., WOJTOWICZ M., LI G.P., *Observing electroluminescence from yellow luminescence-like defects in GaN high electron mobility transistors*, Japanese Journal of Applied Physics **47**(5), 2008, pp. 3336–3339.
[9] TAM S., KO P.K., HU C., *Lucky-electron model of channel hot-electron injection in MOSFET'S*, IEEE Transactions on Electron Devices **31**(9), 1984, pp. 1116–1125.
[10] HUI K., HU C., GEORGE P., KO P.K., *Impact ionization in GaAs MESFETs*, IEEE Electron Device Letters **11**(3), 1990, pp. 113–115.
[11] HSU C.Y., LAN W.H., WU Y.S., *Effect of thermal annealing of Ni/Au ohmic contact on the leakage current of GaN based light emitting diodes*, Applied Physics Letters **83**(12), 2003, pp. 2447–2449.

Received April 12, 2010
in revised form July 27, 2010